Special Issue

Mathematics & Its Relevance to Science and Engineering
Editors: **N. Kishan and K. Phaneendra**

Research Article

Hybrid Nanofluid Flow and Heat Transfer Past a Vertical Cylinder in the Presence of MHD and Heat Generation

V. Rajesh[1] , G. Bala Sowjanya*[1] and Ali Chamkha[2]

[1] *Department of Mathematics, GITAM (deemed to be University), Hyderabad Campus, Rudraram Village, Patancheru (M), Medak, Telangana, India*
[2] *Faculty of Engineering, Kuwait College of Science and Technology, Doha District, Kuwait*
*Corresponding author: gbalasowjanya@gmail.com

Abstract. The basic objective of this work is to investigate the effects of Lorentz force and internal heat generation on the unsteady flow of a hybrid nanofluid and the heat transfer caused by a moving semi-infinite vertical cylinder. The governing partial differential equations are solved numerically using a robust implicit finite difference approach with proper boundary conditions. The current work is corroborated by existing literature on the subject of special situations of the problem. The effects of the magnetic parameter, the Grashof number, and the heat generation parameter on the Nusselt number, the skin friction coefficient, as well as the velocity and temperature fields, have been investigated and graphed. The results obtained can be applied to a variety of engineering devices, such as chemical reactors, heat exchangers, and solar collectors.

Keywords. Free convection, Vertical cylinder, Hybrid nanofluid, MHD, Heat generation, Finite difference numerical method

Mathematics Subject Classification (2020). 80A10, 80A99

1. Introduction

The free convective flow of nanofluids has numerous well-known applications in a variety of sectors. It enhances the heat dissipation capability of electrical equipment. It significantly improves the cooling rate of automotive and heavy-duty engines by increasing efficiency, reducing weight, and simplifying thermal management systems. The use of nanofluids in industrial cooling, nuclear power plant cooling, and solar collectors significantly increases energy savings and pollution reductions. Transient natural convection flow of nanofluids controlled by a magnetic field has captivated the attention of many researchers due to their applications in contemporary materials processing, where magnetic fields are known to achieve exceptional manoeuvrability and control of electrically conducting materials. Magnetohydrodynamic (MHD) convective nanofluid flows also have significant uses in renewable energy devices, such as MHD power generators and nuclear reactor transport operations, where the magnetic field is used to control the rate of heat transfer. Given these uses, much research has been conducted on free convective nanofluid flows to examine heat transfer enhancement; a few of these are listed below (Loganathan *et al.* [14], Rajesh *et al.* [20, 21], Aziz *et al.* [1]). Das *et al.* [6] acknowledge other research on nanofluid convection fluxes, as do Wang and Mujumdar [29–31], Kakaç and Pramuanjaroenkij [11], Kasaeian *et al.* [12], and Lin and Yang [13].

Numerous experiments have been conducted using two different types of nanoparticles suspended in a base fluid dubbed "Hybrid Nanofluid", an advanced nanofluid. The primary advantage of hybrid nanofluid is that, by carefully selecting a good combination of nanoparticles, one may regulate it to enhance the favourable characteristics of each particle type and compensate for the disadvantages of employing them separately due to their synergistic effect. Apart from their high effective thermal conductivity, hybrid nanofluids can provide enormous benefits when nanoparticles are disseminated properly. Nanofluid flow is well-known for its improved heat transfer rate compared to conventional fluid flow. To improve it further, the hybrid nanofluid is pioneered. These hybrid nanofluids may represent a novel class of nanofluids with several potential applications in all disciplines of heat transfer, including microfluidics, manufacturing, transportation, defence, medicine, naval structures, and acoustics. Given these considerations, Suresh *et al.* [25] investigated the two-step production of Al_2O_3–Cu/water hybrid nanofluids and described their thermophysical properties. Later, Suresh *et al.* [24] studied the heat transfer properties of an Al_2O_3–Cu/water hybrid nanofluid. Nine *et al.* [18] described a highly productive method for production and thermal characterization of well-dispersed Cu_2O and Cu/Cu_2O nanoparticles. Momin [16] conducted experimental research of mixed convection using water–Al_2O_3 and a hybrid nanofluid in an inclined tube for laminar flow. Nimmagadda and Venkatasubbaiah [17] investigated microchannel conjugate heat transfer employing innovative hybrid nanofluids (Al_2O_3 + Ag/water). Sarkar *et al.* [22] discussed the history of hybrid nanofluids and their applications. Several other studies on hybrid nanofluids are discussed by Takabi *et al.* [26]; Devi and Devi [7]; Ranga Babu *et al.* [2], Olatundun and

Makinde [19], Gorla *et al.* [9], Mehryan *et al.* [15], Chamkha *et al.* [5], Hayat and Nadeem [10], and Tayebi and Chamkha [27].

Motivated by the aforementioned papers and applications in engineering and industry, the purpose of this paper is to investigate the two-dimensional unsteady free convective laminar boundary layer flow of a viscous incompressible electrically conducting Cu–Al$_2$O$_3$/water hybrid nanofluid caused by a moving semi-infinite vertical cylinder. The purpose of this study is to investigate the effects of Lorentz force, internal heat generation, Grashof number, and fluid type on the Nusselt number, skin friction coefficient, temperature, and velocity profiles.

Nomenclature

t	=	Dimensionless time;
Pr	=	Prandtl number;
Gr	=	Thermal Grashof number;
g	=	Acceleration due to the gravity (m s^{-2});
κ	=	Thermal conductivity (J m^{-1} K^{-1});
θ_∞^*	=	Temperature of the fluid far away from the cylinder;
θ^*	=	Temperature of the fluid (K);
θ_w^*	=	Temperature of the cylinder;
C_p	=	Specific heat at constant pressure (J kg^{-1} K^{-1});
δ_2	=	Solid volume fraction of Al$_2$O$_3$ nanoparticles;
C_f	=	Skin friction coefficient;
r_0	=	Radius of the cylinder (m);
r^*	=	Radial coordinate normal to the cylinder (m);
Nu$_x$	=	Local Nusselt number;
μ	=	Dynamic viscosity (Pa s);
u_1	=	Dimensionless velocity component in the x-direction;
u_2	=	Dimensionless velocity component in the r-direction;
r	=	Dimensionless radial coordinate normal to the cylinder;
δ_1	=	Solid volume fraction of Cu nanoparticles;
n_1	=	Empirical shape factor for the nanoparticle;
Al$_2$O$_3$	=	Aluminium oxide;
β	=	Volumetric thermal expansion coefficient (K^{-1});
u_1^*	=	Velocity component in the x-direction (m s^{-1});
u_2^*	=	Velocity component in the r-direction (m s^{-1});
t^*	=	Time (s);
x^*	=	Spatial coordinate along the cylinder (m);
ν	=	Kinematic viscosity (m^2 s^{-1});

Δt	=	Grid size in the time;
Δr	=	Grid size in the radial direction;
Δx	=	Grid size in the axial direction;
θ	=	Dimensionless temperature;
x	=	Dimensionless spatial coordinate along the cylinder;
ρ	=	Density (kg m^{-3});
Cu	=	Copper

Subscripts

w	=	Conditions on the wall;
$s2$	=	Solid nanoparticles of Al_2O_3;
nf	=	Nanofluid;
hnf	=	Hybrid nanofluid;
i	=	Grid point along the x-direction;
j	=	Grid point along the r-direction;
∞	=	Free stream condition;
$s1$	=	Solid nanoparticles of Cu;
f	=	Base fluid

Superscripts

n	=	Grid point along the t-direction

2. Mathematical Model

The physical model and coordinate system used in this work are depicted in Figure 1. Both the cylinder and the fluid are initially stationary and have a free stream temperature of θ_∞^* at $t^* \leq 0$. Following that, at time $t^* > 0$, the cylinder begins to move with a uniform velocity u_0. The temperature at the surface is increased to θ_w^*. We assume that a constant magnetic field of intensity B_0 acts in the radial direction and that the resultant induced magnetic field is insignificant, which is feasible when the magnetic Reynolds number is low. It is assumed that the viscous dissipation, Ohmic heating, ion-slip, and Hall effects are negligible. Copper (Cu) and aluminium oxide Al_2O_3 nanoparticles with water as the base fluid are investigated in this analysis. Initially, in this problem, a Cu/water nanofluid is generated by scattering Cu nanoparticles with a volume fraction of 0.1 vol. solid (which remains constant throughout the problem) into the base fluid, i.e., water. Then, varied volume fractions of Al_2O_3 nanoparticles are distributed in Cu/water nanofluid to create the desired hybrid nanofluid Cu–Al_2O_3/water. The system is axisymmetric. Table 1 summarises the nanoparticles' thermophysical characteristics. According to Tiwari and Das's [28] nanofluid model and Boussinesq approximation [23], the governing equations that control the flow are as follows:

Continuity equation:

$$\frac{\partial(r^* u_1^*)}{\partial x^*} + \frac{\partial(r^* u_2^*)}{\partial r^*} = 0 \tag{2.1}$$

Momentum equation

$$\frac{\partial u_1^*}{\partial t^*} + u_1^* \frac{\partial u_1^*}{\partial x^*} + u_2^* \frac{\partial u_1^*}{\partial r^*} = \nu_{hnf} \frac{1}{r^*} \frac{\partial}{\partial r^*} \left(r^* \frac{\partial u_1^*}{\partial r^*} \right) + \frac{(\rho\beta)_{hnf}}{\rho_{hnf}} g(\theta^* - \theta_\infty^*) - \frac{\sigma_{hnf} B_0^2 u_1^*}{\rho_{hnf}} \tag{2.2}$$

Energy equation

$$\frac{\partial\theta^*}{\partial t^*} + u_1^* \frac{\partial\theta^*}{\partial x^*} + u_2^* \frac{\partial\theta^*}{\partial r^*} = \frac{\kappa_{hnf}}{(\rho C_p)_{hnf}} \frac{1}{r^*} \frac{\partial}{\partial r^*} \left(r^* \frac{\partial\theta^*}{\partial r^*} \right) + \frac{Q_0}{(\rho C_p)_{hnf}} (\theta^* - \theta_\infty^*) \tag{2.3}$$
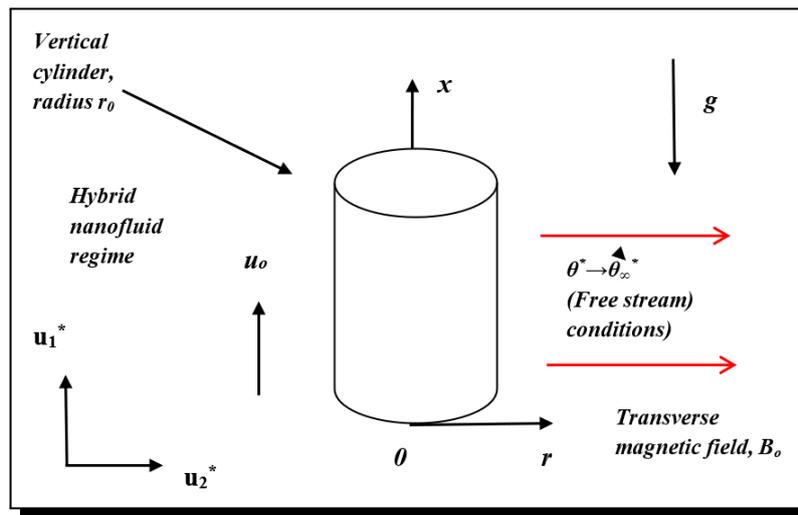
Figure 1. The physical model and coordinate system

The initial and boundary conditions are

$$t^* \leq 0 : u_1^* = 0, \quad u_2^* = 0, \ \theta^* = \theta_\infty^* \quad \text{for all } x^* \geq 0 \text{ and } r^* \geq 0$$

$$t^* > 0 : u_1^* = u_0, \ u_2^* = 0, \ \theta^* = \theta_w^* \quad \text{at } r^* = r_0$$

$$u_1^* = 0, \ \theta^* = \theta_\infty^* \quad \text{at } x^* = 0 \text{ and } r^* \geq r_0$$

$$u_1^* \to 0, \ \theta^* \to \theta_\infty^* \quad \text{as } r^* \to \infty \tag{2.4}$$

For hybrid nanofluid, the expressions of density ρ_{hnf}, dynamic viscosity μ_{hnf}, heat capacity $(\rho C_P)_{hnf}$, thermal expansion coefficient $(\rho\beta)_{hnf}$, thermal conductivity κ_{hnf}, electrical conductivity σ_{hnf} are respectively given by

$$\rho_{hnf} = [(1-\delta_2)\{(1-\delta_1)\rho_f + \delta_1\rho_{s1}\}] + \delta_2\rho_{s2},$$

$$\mu_{hnf} = \frac{\mu_f}{(1-\delta_1)^{2.5}(1-\delta_2)^{2.5}},$$

$$(\rho C_P)_{hnf} = [(1-\delta_2)\{(1-\delta_1)(\rho C_P)_f + \delta_1(\rho C_P)_{s1}\}] + \delta_2(\rho C_P)_{s2},$$

$$(\rho\beta)_{hnf} = [(1-\delta_2)\{(1-\delta_1)(\rho\beta)_f + \delta_1(\rho\beta)_{s1}\}] + \delta_2(\rho\beta)_{s2},$$

$$\kappa_{hnf} = \kappa_{bf} \frac{\kappa_{s2} + (n_1-1)\kappa_{bf} - (n_1-1)\delta_2(\kappa_{bf} - \kappa_{s2})}{\kappa_{s2} + (n_1-1)\kappa_{bf} + \delta_2(\kappa_{bf} - \kappa_{s2})}.$$

where

$$\kappa_{bf} = \kappa_f \frac{\kappa_{s1} + (n_1 - 1)\kappa_f - (n_1 - 1)\delta_1(\kappa_f - \kappa_{s1})}{\kappa_{s1} + (n_1 - 1)\kappa_f + \delta_1(\kappa_f - \kappa_{s1})},$$

$$\sigma_{hnf} = \sigma_{bf} \left[\frac{\sigma_{s2}(1 + 2\delta_2) + 2\sigma_{bf}(1 - \delta_2)}{\sigma_{s2}(1 - \delta_2) + \sigma_{bf}(2 + \delta_2)} \right],$$

wherein

$$\sigma_{bf} = \sigma_f \left[\frac{\sigma_{s1}(1 + 2\delta_1) + 2\sigma_f(1 - \delta_1)}{\sigma_{s1}(1 - \delta_1) + \sigma_f(2 + \delta_1)} \right]. \tag{2.5}$$

Table 1. Thermophysical properties of water and nanoparticles

	ρ (kg/m^3)	C_p (J/kg K)	κ (W/m K)	σ (s/m)	β (1/K)
$H_2O(f)$	997.1	4179	0.613	5.5×10^{-6}	21×10^{-5}
$Al_2O_3(s2)$	3970	765	40	35×10^6	0.85×10^{-5}
$Cu(s1)$	8933	385	401	59.6×10^6	1.67×10^{-5}

Using the following transformations

$$u_1 = \frac{u_1^*}{u_0}, \ u_2 = \frac{u_2^* r_0}{\nu_f}, \ x = \frac{x^* \nu_f}{u_0 r_0^2}, \ r = \frac{r^*}{r_0}, \ t = \frac{t^* \nu_f}{r_0^2}, \ \theta = \frac{\theta^* - \theta_\infty^*}{\theta_w^* - \theta_\infty^*} \tag{2.6}$$

into equations (2.1), (2.2) and (2.3) we get

$$\frac{\partial u_1}{\partial x} + \frac{\partial u_2}{\partial r} + \frac{u_2}{r} = 0, \tag{2.7}$$

$$\frac{\partial u_1}{\partial t} + u_1 \frac{\partial u_1}{\partial x} + u_2 \frac{\partial u_1}{\partial r} = \frac{E_2}{E_1} \frac{1}{r} \frac{\partial}{\partial r}\left(r \frac{\partial u_1}{\partial r}\right) + \frac{E_3}{E_1} Gr\theta - \frac{E_4}{E_1} Mu_1, \tag{2.8}$$

$$\frac{\partial \theta}{\partial t} + u_1 \frac{\partial \theta}{\partial x} + u_2 \frac{\partial \theta}{\partial r} = \frac{E_6}{E_5} \frac{1}{P_r} \frac{1}{r} \frac{\partial}{\partial r}\left(r \frac{\partial \theta}{\partial r}\right) + \frac{Q}{E_5} \theta. \tag{2.9}$$

The corresponding initial and boundary conditions are

$$t \leq 0 : u_1 = 0, \ u_2 = 0, \ \theta = 0 \text{ for all } x \text{ and } r$$

$$t > 0 : u_1 = 1, \ u_2 = 0, \ \theta = 1 \text{ at } r = 1$$

$$u_1 = 0, \ \theta = 0 \text{ at } x = 0$$

$$u_1 \to 0, \ \theta \to 0 \text{ as } r \to \infty \tag{2.10}$$

where

$$\Pr = \frac{\nu_f}{\alpha_f} \text{ (Prandtl number)},$$

$$Gr = \frac{g\beta_f r_0^2(\theta_w^* - \theta_\infty^*)}{u_0 \nu_f} \text{ (Grashof number)},$$

$$M = \frac{\sigma_f B_0^2 r_0^2}{\rho_f \nu_f} \text{ (Magnetic parameter)},$$

$$Q = \frac{Q_0 r_0^2}{(\mu C_p)_f} \text{ (Heat generation parameter)},$$

and

$$E_1 = \left[(1-\delta_2)\left\{(1-\delta_1)+\delta_1\frac{\rho_{s1}}{\rho_f}\right\}\right] + \delta_2\frac{\rho_{s2}}{\rho_f}, \quad E_2 = \frac{1}{(1-\delta_1)^{2.5}(1-\delta_2)^{2.5}},$$

$$E_3 = \left[(1-\delta_2)\left\{(1-\delta_1)+\delta_1\frac{(\rho\beta)_{s1}}{(\rho\beta)_f}\right\}\right] + \delta_2\frac{(\rho\beta)_{s2}}{(\rho\beta)_f},$$

$$E_4 = \frac{\sigma_{bf}}{\sigma_f}\left[\frac{\sigma_{s2}(1+2\delta_2)+2\sigma_{bf}(1-\delta_2)}{\sigma_{s2}(1-\delta_2)+\sigma_{bf}(2+\delta_2)}\right],$$

$$E_5 = \left[(1-\delta_2)\left\{(1-\delta_1)+\delta_1\frac{(\rho C_p)_{s1}}{(\rho C_p)_f}\right\}\right] + \delta_2\frac{(\rho C_p)_{s2}}{(\rho C_p)_f},$$

$$E_6 = \frac{\kappa_{bf}}{\kappa_f}\frac{[\kappa_{s2}+(n_1-1)\kappa_{bf}-(n_1-1)\delta_2(\kappa_{bf}-\kappa_{s2})]}{[\kappa_{s2}+(n_1-1)\kappa_{bf}+\delta_2(\kappa_{bf}-\kappa_{s2})]}. \tag{2.11}$$

3. Numerical Method and its Validation

The equations (2.7)-(2.9) with conditions(2.10) are solved using an unconditionally stable finite-difference numerical approach of the Crank-Nicolson type. The associated finite-difference equations are as follows:

$$\left[\frac{(u_1)_{i,j}^{n+1}-(u_1)_{i-1,j}^{n+1}+(u_1)_{i,j}^{n}-(u_1)_{i-1,j}^{n}+(u_1)_{i,j-1}^{n+1}-(u_1)_{i-1,j-1}^{n+1}+(u_1)_{i,j-1}^{n}-(u_1)_{i-1,j-1}^{n}}{4\Delta x}\right]$$

$$+\left[\frac{(u_2)_{i,j}^{n+1}-(u_2)_{i,j-1}^{n+1}+(u_2)_{i,j}^{n}-(u_2)_{i,j-1}^{n}}{2\Delta r}\right]+\left[\frac{(u_2)_{i,j}^{n+1}}{1+(j-1)\Delta r}\right]=0, \tag{3.1}$$

$$\left[\frac{(u_1)_{i,j}^{n+1}-(u_1)_{i,j}^{n}}{\Delta t}\right]+(u_1)_{i,j}^{n}\left[\frac{(u_1)_{i,j}^{n+1}-(u_1)_{i-1,j}^{n+1}+(u_1)_{i,j}^{n}-(u_1)_{i-1,j}^{n}}{2\Delta x}\right]$$

$$+(u_2)_{i,j}^{n}\left[\frac{(u_1)_{i,j+1}^{n+1}-(u_1)_{i,j-1}^{n+1}+(u_1)_{i,j+1}^{n}-(u_1)_{i,j-1}^{n}}{4\Delta r}\right]$$

$$=\frac{E_3}{E_1}\frac{G_r}{2}[\theta_{i,j}^{n+1}+\theta_{i,j}^{n}]+\frac{E_2}{E_1}\left[\frac{(u_1)_{i,j-1}^{n+1}-2(u_1)_{i,j}^{n+1}+(u_1)_{i,j+1}^{n+1}+(u_1)_{i,j-1}^{n}-2(u_1)_{i,j}^{n}+(u_1)_{i,j+1}^{n}}{2(\Delta r)^2}\right]$$

$$+\frac{E_2}{E_1}\left[\frac{(u_1)_{i,j+1}^{n+1}-(u_1)_{i,j-1}^{n+1}+(u_1)_{i,j+1}^{n}-(u_1)_{i,j-1}^{n}}{4[1+(j-1)\Delta r]\Delta r}\right]-\frac{E_4}{E_1}\frac{M}{2}[(u_1)_{i,j}^{n+1}+(u_1)_{i,j}^{n}], \tag{3.2}$$

$$\left[\frac{\theta_{i,j}^{n+1}-\theta_{i,j}^{n}}{\Delta t}\right]+(u_1)_{i,j}^{n}\left[\frac{\theta_{i,j}^{n+1}-\theta_{i-1,j}^{n+1}+\theta_{i,j}^{n}-\theta_{i-1,j}^{n}}{2\Delta x}\right]+(u_2)_{i,j}^{n}\left[\frac{\theta_{i,j+1}^{n+1}-\theta_{i,j-1}^{n+1}+\theta_{i,j+1}^{n}-\theta_{i,j-1}^{n}}{4\Delta r}\right]$$

$$=\frac{E_6}{E_5}\left[\frac{\theta_{i,j-1}^{n+1}-2\theta_{i,j}^{n+1}+\theta_{i,j+1}^{n+1}+\theta_{i,j-1}^{n}-2\theta_{i,j}^{n}+\theta_{i,j+1}^{n}}{2\Pr(\Delta r)^2}\right]+\frac{Q}{2E_5}[\theta_{i,j}^{n+1}+\theta_{i,j}^{n}]$$

$$+\frac{E_6}{E_5}\left[\frac{\theta_{i,j+1}^{n+1}-\theta_{i,j-1}^{n+1}+\theta_{i,j+1}^{n}-\theta_{i,j-1}^{n}}{4\Pr[1+(j-1)\Delta r]\Delta r}\right]. \tag{3.3}$$

Rajesh *et al.* [20] and Ganesan and Rani [8] provide details on solving the finite difference equations for velocity and temperature profiles using the Thomas technique [3]. Additionally, during this early transient regime, the heat transfer process is dominated by pure heat conduction. Thus, the early temperature distribution is analogous to the transient conduction problem in a semi-infinite material. The transient temperature distribution in a semi-infinite material is given by the following equation (Schlichting and Gersten [23], and Carslaw and Jaeger [4])

$$\theta = r^{-1/2} erfc\left(\frac{r-1}{2\sqrt{t/\mathrm{Pr}}}\right) \tag{3.4}$$

with the initial and boundary conditions:

$$t \le 0 : \theta = 0 \text{ for all } r$$

$$t > 0 : \theta = 1 \text{ at } r = 1 \tag{3.5}$$

To support the current investigation, Figure 2 compares transient temperature profiles generated using eq. (3.4) to the current profiles in the absence of the heat generation parameter (where $\delta_1 = 0$, $\delta_2 = 0$) at two distinct early periods. They are shown to be in great agreement, demonstrating the validity of the present numerical technique for this class of unsteady flow problems.
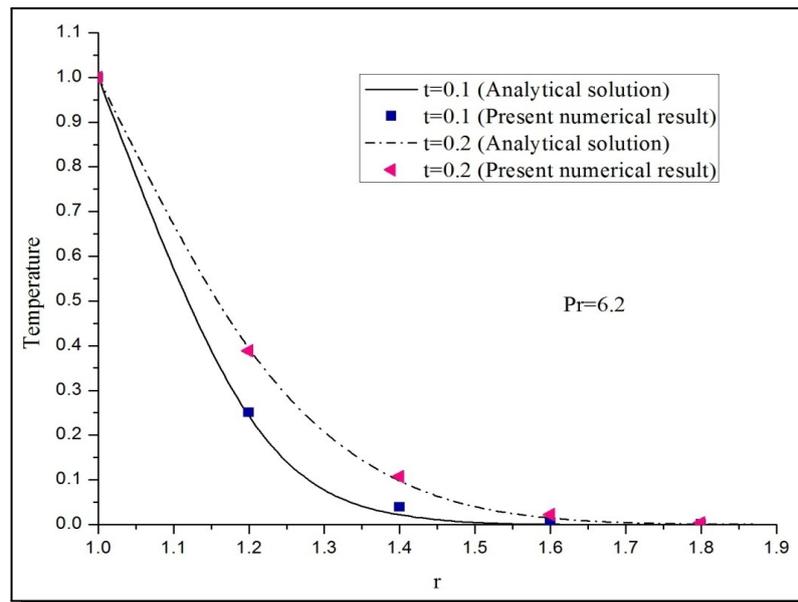
Figure 2. Comparison of temperature profiles

4. Engineering Quantities

Numerous physical quantities are relevant in industrial materials processing, for example, the skin friction coefficient C_f and the local Nusselt number Nu_x, which are defined as follows:

$$C_f = \frac{\tau_w}{\rho_f u_0^2}, \quad \mathrm{Nu}_x = \frac{q_w x^*}{\kappa_f(\theta_w^* - \theta_\infty^*)}. \tag{4.1}$$

Here, τ_w denotes skin friction and q_w denotes the rate of heat transfer from the cylinder's surface, which are defined as follows:

$$\tau_w = \mu_{hnf}\left(\frac{\partial u_1^*}{\partial r^*}\right)_{r^*=r_0}, \quad q_w = -\kappa_{hnf}\left(\frac{\partial \theta^*}{\partial r^*}\right)_{r^*=r_0}. \tag{4.2}$$

Using non-dimensional variables (2.6), we get

$$\operatorname{Re} C_f = \frac{1}{(1-\delta_1)^{2.5}(1-\delta_2)^{2.5}}\left(\frac{\partial u_1}{\partial r}\right)_{r=1}, \quad \operatorname{Re}^{-1}\operatorname{Nu}_x = -\frac{\kappa_{hnf}}{\kappa_f}x\left(\frac{\partial \theta}{\partial r}\right)_{r=1}. \tag{4.3}$$

Here $\operatorname{Re} = \frac{u_0 r_0}{v_f}$ is the Reynolds number. In eq. (4.3), the derivatives are evaluated using a five-point approximation formula.

5. Results and Discussion

To visualise the physics of the problem, Figures 3-22 depict a graphical study of the flow and heat transfer characteristics for various regulating factors. The current study addressed spherical nanoparticles ($n_1 = 3$). The basic fluid's Prandtl number, Pr, is maintained constant at 6.2. When $\delta_2 = 0$, the present model simplifies to the governing equations for the Cu/water nanofluid. When both $\delta_1 = 0$ and $\delta_2 = 0$ are present, the model is reduced to the governing equations for a standard viscous fluid, i.e., nanoscale properties are eliminated. Figure 3 illustrates the effect of the magnetic parameter (M) on the velocity field. Lorentz force is produced when a transverse magnetic field interacts with an electric field during the motion of an electrically conducting fluid. It is discovered that as the magnetic field intensity increases for both nanofluid and hybrid nanofluid, the retarding force increases and, as a result, the velocity decreases along with the thickness of the momentum boundary layer. However, the magnetic parameter (M) has a minor effect on the temperature field, as illustrated in Figure 4. According to Figure 5, as the flow velocity is reduced due to the building magnetic field, the skin friction decreases for both nanofluid and hybrid nanofluid. As the magnetic parameter increases, the Nusselt number, which represents the non-dimensional heat transfer rate, decreases, as illustrated in Figure 6.
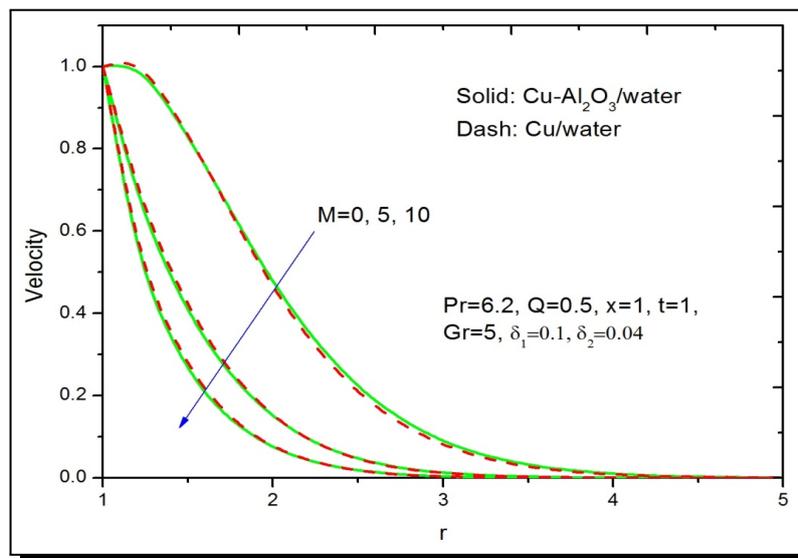
Figure 3. Effect of M on velocity profiles
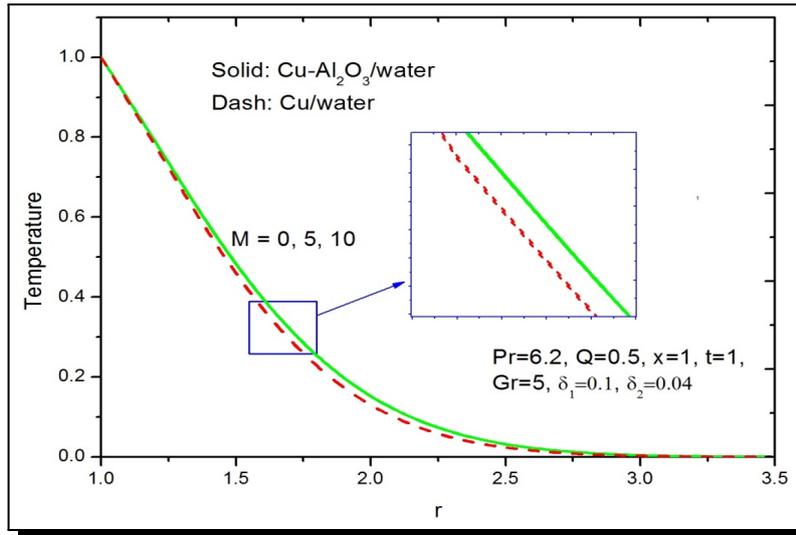
Figure 4. Effect of M on temperature profiles
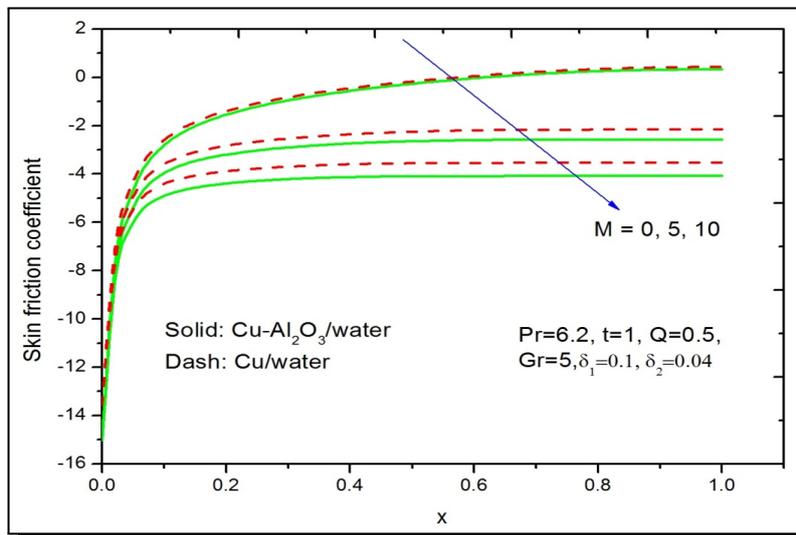
Figure 5. Effect of M on skin friction coefficient
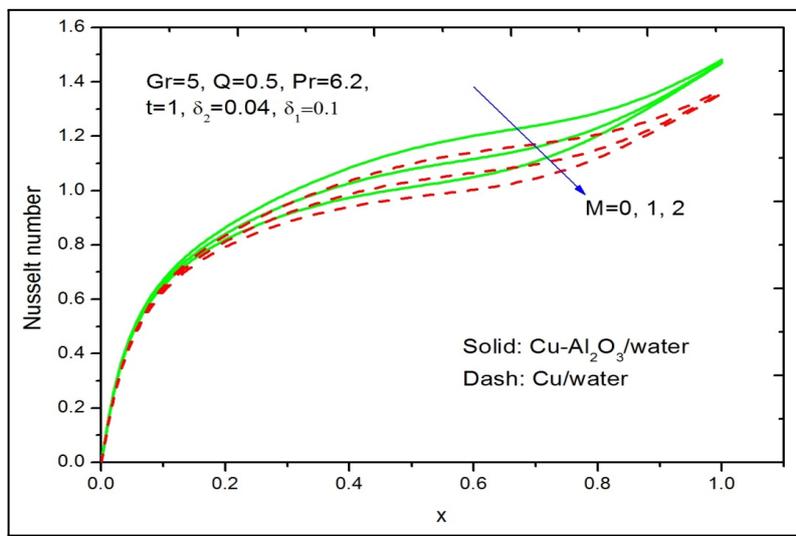
Figure 6. Effect of M on Nusselt number

Figures 7 and 8 illustrate the effect of the Grashof number on the velocity and temperature distributions, respectively. As the Grashof number increases, the thermal buoyancy force increases, hence increasing the velocity, as illustrated in Figure 7. As illustrated in Figure 8, an increase in Gr results in a decrease in temperature because an increase in buoyant force results in a decrease in thermal diffusion. As the flow velocity increases due to the increasing Grashof number, the skin friction coefficient increases as well, as illustrated in Figure 9. Additionally, as the Grashof number increases, the non-dimensional heat transfer rate increases for both the hybrid nanofluid and nanofluid.
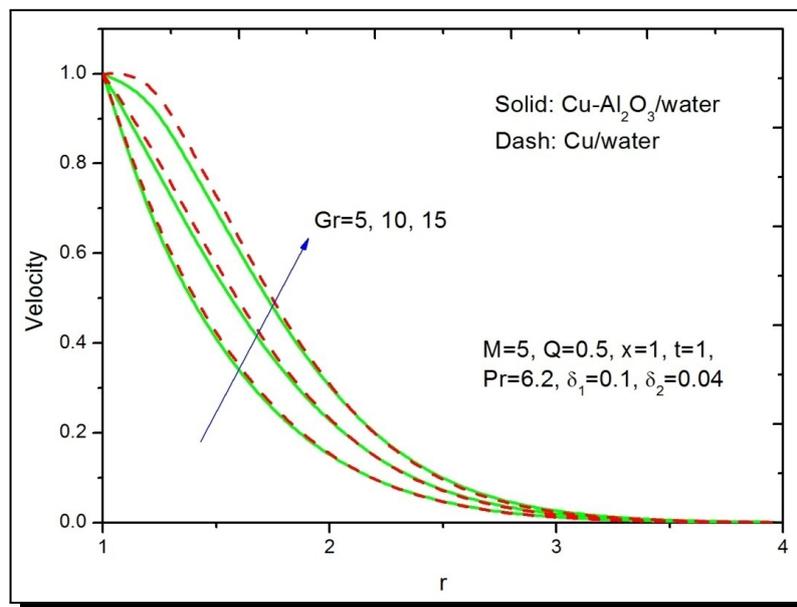
Figure 7. Effect of Gr on velocity profiles
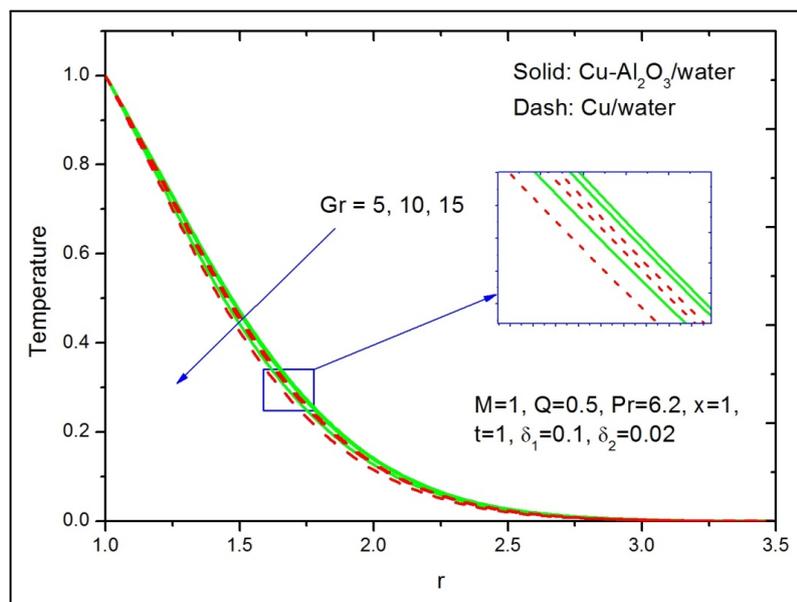
Figure 8. Effect of Gr on temperature profiles
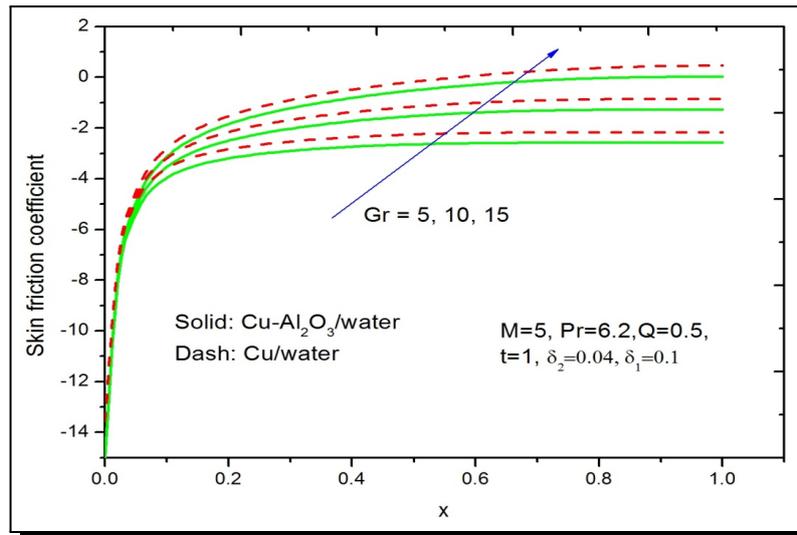
Figure 9. Effect of Gr on skin friction coefficient
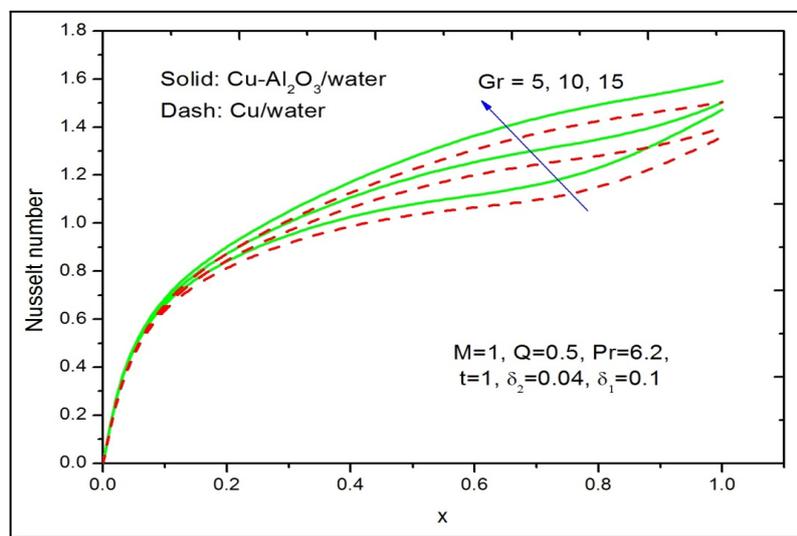
Figure 10. Effect of Gr on Nusselt number

Figures 11 and 12 illustrate how the regulation of heat generation affects the velocity and temperature distributions. When heat is generated, the buoyancy force increases, resulting in increased boundary layer velocities. As a result, the velocity of fluid flow increases in proportion to the increasing heat generation parameter, as illustrated in Figure 11 for both hybrid nanofluid and nanofluid. When heat is generated in the fluid, one would predict an increase in the temperature of the thermal boundary layer. This is demonstrated in Figure 12, where temperatures increase as the heat generation parameter increases for both hybrid nanofluid and nanofluid. Because the velocity of the flow increases as the heat generation parameter is increased, the skin friction coefficient increases for both hybrid nanofluid and nanofluid, as illustrated in Figure 13. Additionally, as illustrated in Figure 14, the rate of heat transmission decreases dramatically for both the hybrid nanofluid and nanofluid when the heat generating parameter is increased.
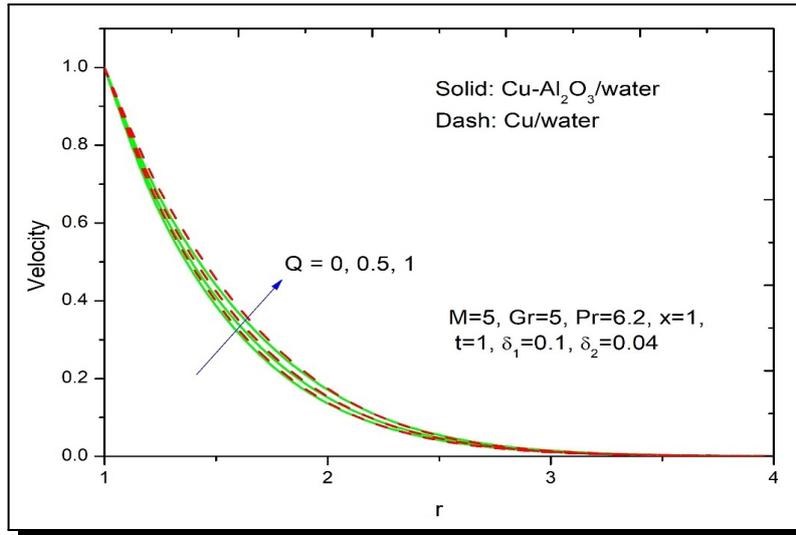
Figure 11. Effect of Q on velocity profiles
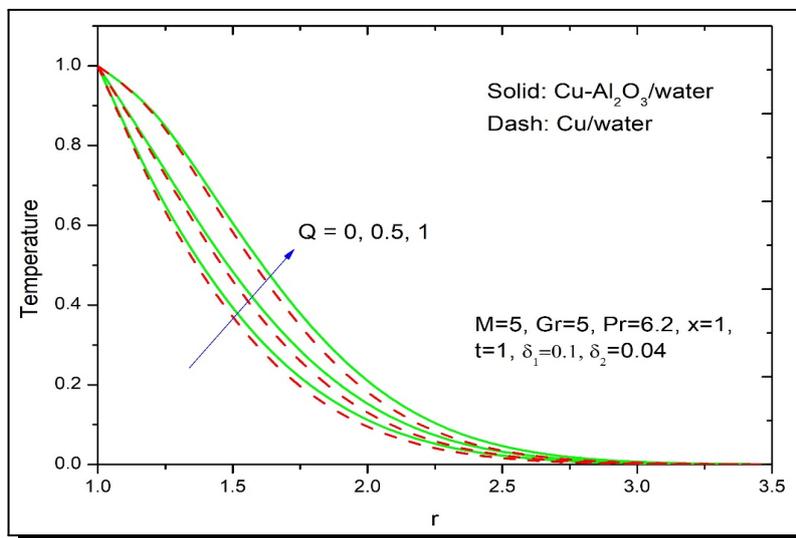
Figure 12. Effect of Q on temperature profiles
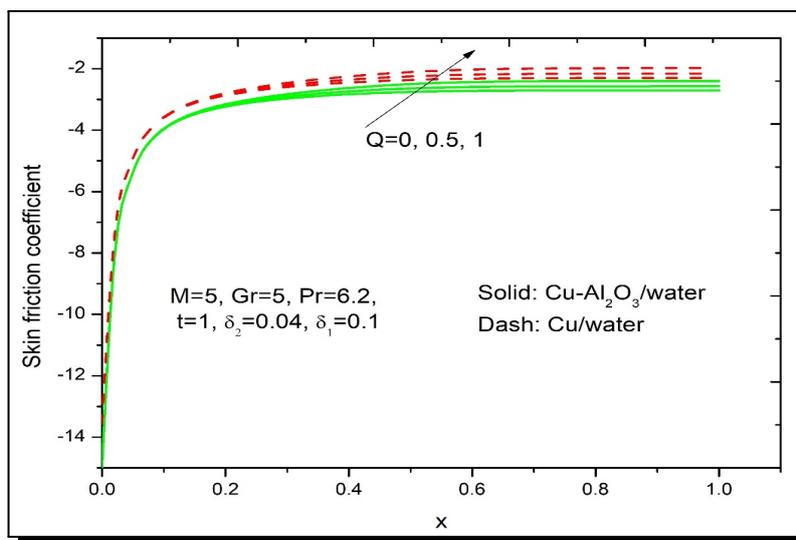
Figure 13. Effect of Q on skin friction coefficient
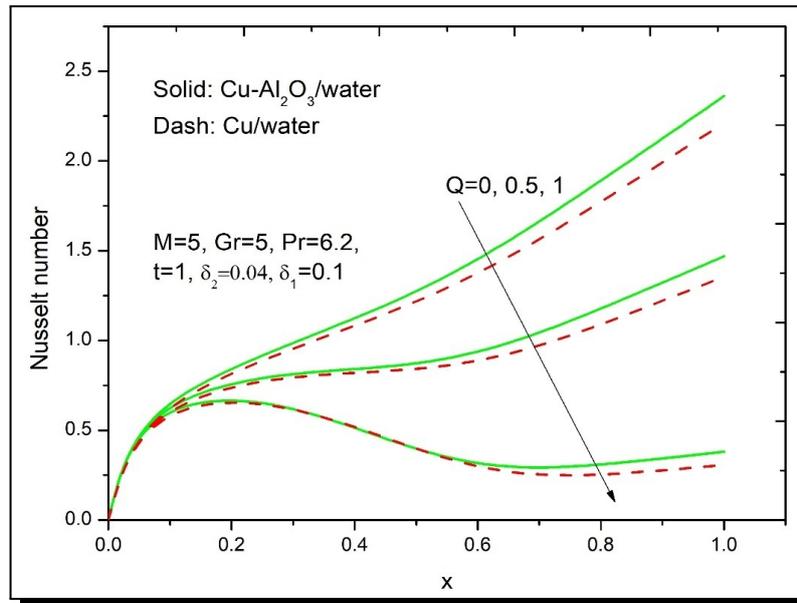
Figure 14. Effect of Q on Nusselt number

Figures 15 and 16 show the velocity and temperature curves with increased time for both hybrid nanofluid and nanofluid. As time progresses, velocity increases for both hybrid nanofluid and nanofluid, along with the thickness of the momentum boundary layer, as illustrated in Figure 15. As with the velocity field, it is apparent from Figure 16 that the temperature and its boundary layer thickness increase with rising time. Additionally, it is apparent from Figure 17 that as time progresses, the skin friction coefficient increases. This is due to the fact that velocity increases with time. The rate of non-dimensional heat transmission is observed to decrease with increasing time, as illustrated in Figure 18.
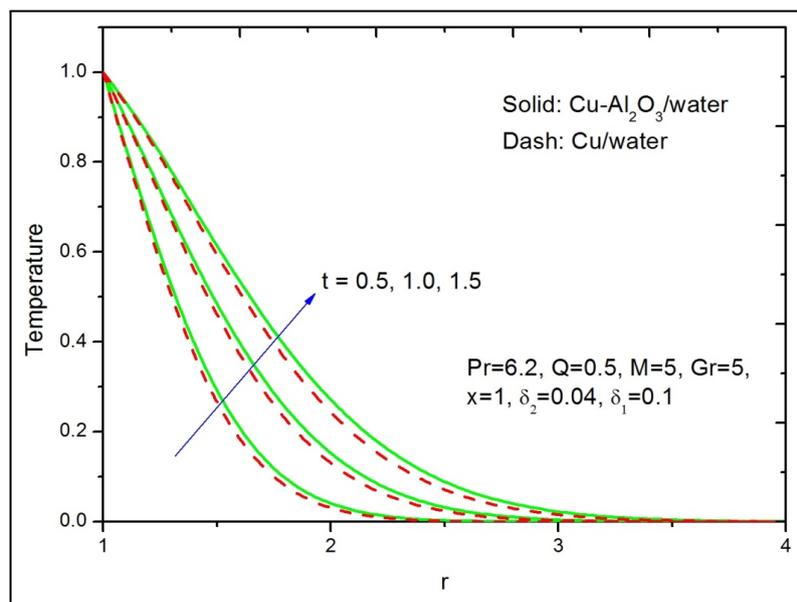
Figure 15. Development of velocity profiles with a time
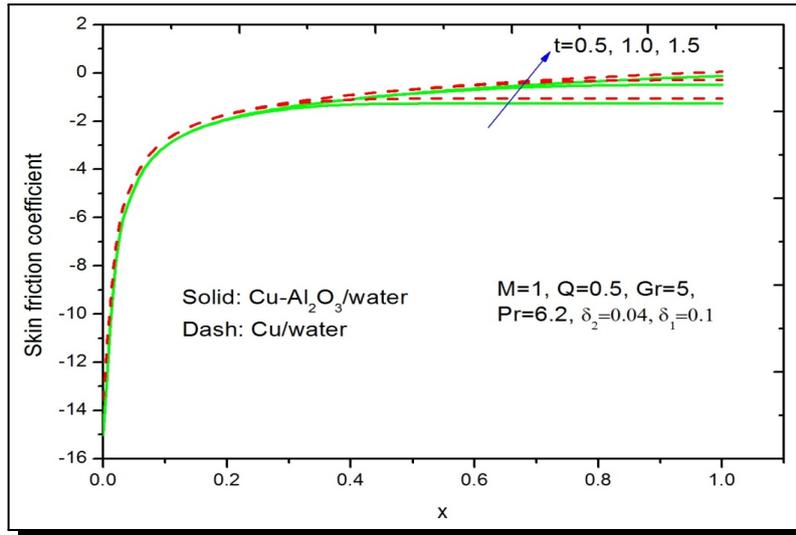
Figure 16. Development of temperature profiles with a time
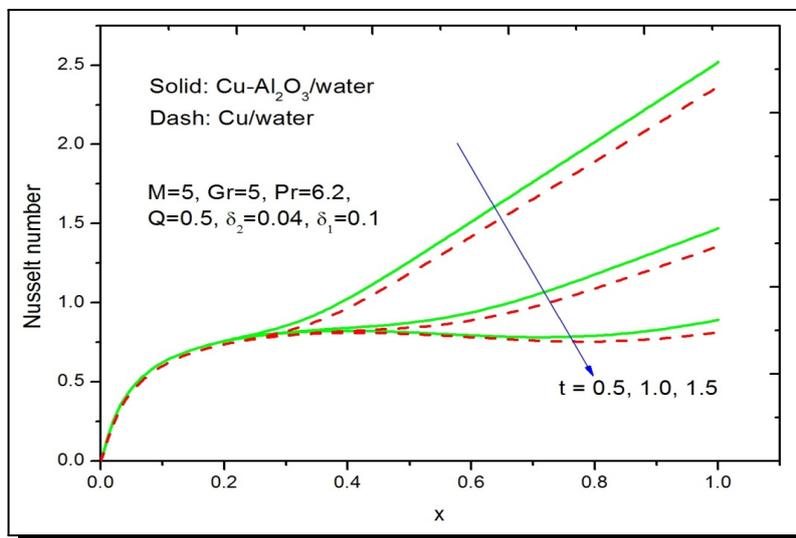
Figure 17. Effect of time t on the skin friction coefficient
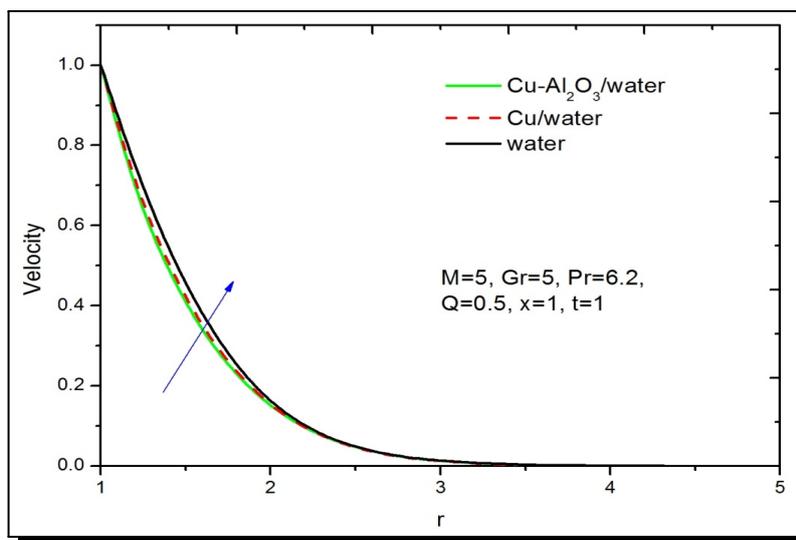
Figure 18. Effect of time t on Nusselt number

Figures 19 and 20 compare the velocity and temperature distributions of pure water, nanofluid (Cu/water), and hybrid nanofluid (Cu–Al$_2$O$_3$/water). As illustrated in Figure 19, the hybrid nanofluid (Cu–Al$_2$O$_3$/water) flow has a lower velocity than nanofluid (Cu/water) and pure water flows. As illustrated in Figure 20, the hybrid nanofluid (Cu–Al$_2$O$_3$/water) obtains a greater temperature than purewater and nanofluid (Cu/water). Due to the slower flow velocity of the hybrid nanofluid, the skin friction coefficient is discovered to be less than that of nanofluid and pure water, which is transparent in Figure 21. Additionally, Figure 22 demonstrates that the non-dimensional heat transfer rate through Cu–Al$_2$O$_3$/water is greater than the rate through (Cu/water). A similar occurrence is felt when the magnetic parameter, the Grashof number, the heat generation parameter, and also the time parameter are increased, as illustrated in Figures 6, 10, 14, and 18. Thus, the necessary heat transfer rate can be accomplished by selecting diverse and suitable nanoparticle proportions in hybrid nanofluid.
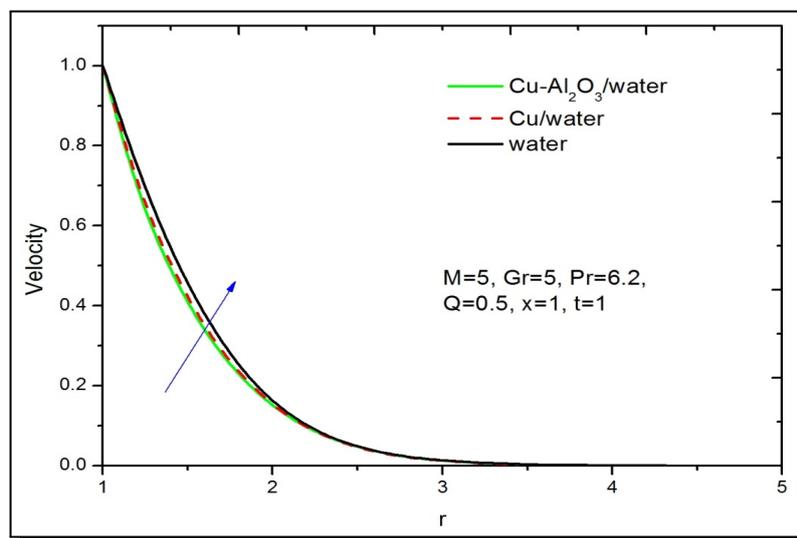
Figure 19. Velocity profiles of water, nanofluid and hybrid nanofluid
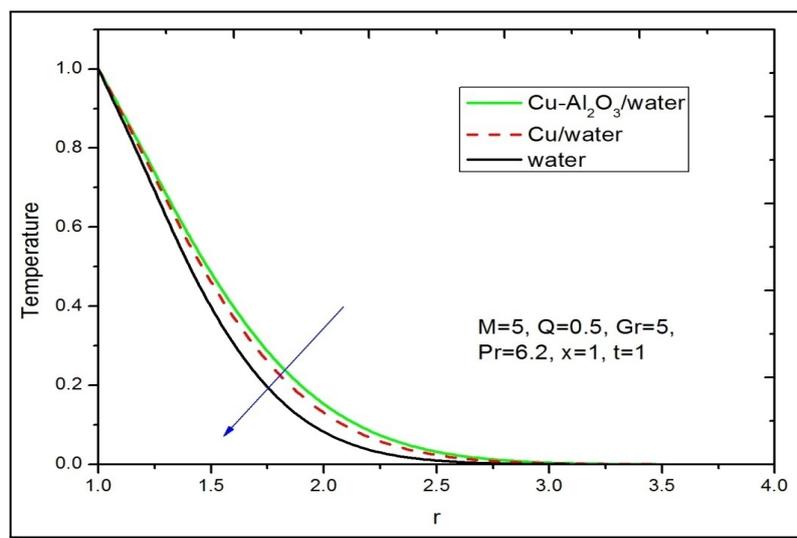
Figure 20. Temperature profiles of water, nanofluid and hybrid nanofluid
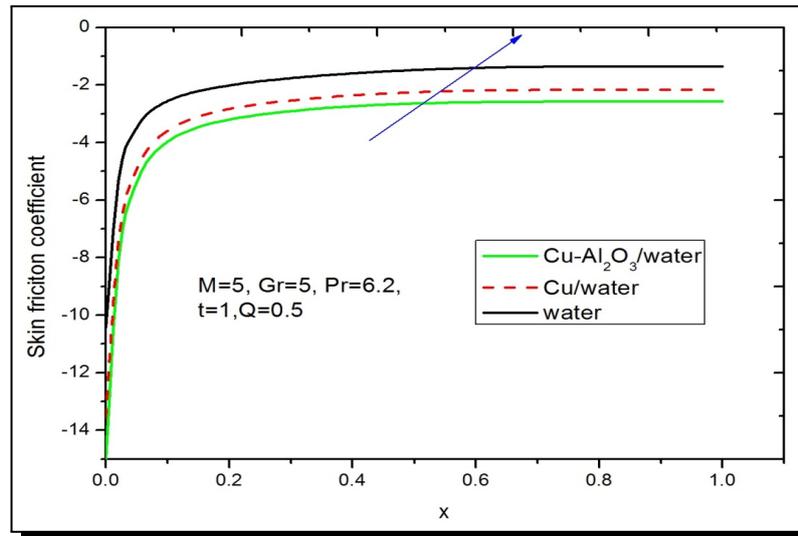
Figure 21. Skin friction coefficients of water, nanofluid and hybrid nanofluid
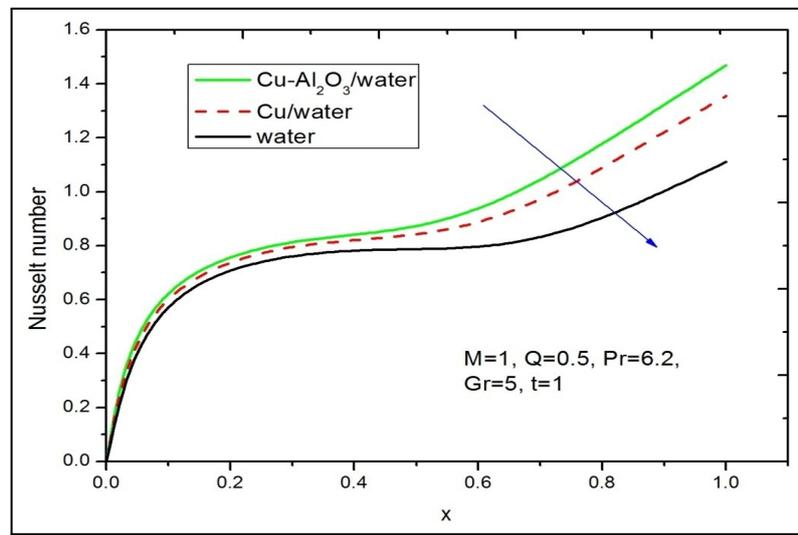
Figure 22. Nusselt numbers of water, nanofluid and hybrid nanofluid

6. Conclusions

The article analyses numerically the effect of MHD and internal heat generation on the transient free convective flow of a hybrid nanofluid (Cu–Al_2O_3/water) past a moving vertical cylinder. The dimensionless flow and heat transfer regulating equations are solved using a finite difference technique of the Crank-Nicolson type. The following closing remarks are derived from the graphical representation:

(1) As the magnetic parameter is increased, the hybrid nanofluid (Cu–Al_2O_3/water) flow velocity decreases, as does the thickness of the momentum barrier layer.

(2) As the magnetic parameter is increased, the skin friction coefficient and rate of heat transfer of the hybrid nanofluid (Cu–Al_2O_3/water) decrease.

(3) Increasing the Grashof number decreases the temperature of the hybrid nanofluid (Cu–Al$_2$O$_3$/water) and increases its velocity.

(4) The skin friction coefficient and the rate of heat transfer via the hybrid nanofluid (Cu–Al$_2$O$_3$/water) increase as the Grashof number increases.

(5) As the heat generation parameter increases, the velocity and temperature of the hybrid nanofluid (Cu–Al$_2$O$_3$/water) flow magnify.

(6) As the heat generating parameter increases, the skin friction coefficient increases while the rate of heat transfer decreases dramatically for the hybrid nanofluid (Cu–Al$_2$O$_3$/water).

(7) By using Cu–Al$_2$O$_3$/water as the working fluid, it is possible to obtain higher temperatures and lower velocities than those associated with Cu/water.

(8) By using Cu–Al$_2$O$_3$/water as the working fluid, it is possible to achieve a higher heat transfer rate and a lower skin friction coefficient than those associated with Cu/water.

Competing Interests

The authors declare that they have no competing interests.

Authors' Contributions

All the authors contributed significantly in writing this article. The authors read and approved the final manuscript.

References

[1] A. Aziz, A. Alsaedi, T. Muhammad and T. Hayat, Numerical study for heat generation/absorption in flow of nanofluid by a rotating disk, *Results in Physics* **8** (2018), 785 – 792, DOI: 10.1016/j.rinp.2018.01.009.

[2] J. A. R. Babu, K. K. Kumar and S. S. Rao, State-of-art review on hybrid nanofluids, *Renewable and Sustainable Energy Reviews* **77** (2017), 551 – 565, DOI: 10.1016/j.rser.2017.04.040.

[3] B. Carnahan, H. A. Luther and J. O. Wilkes, *Applied Numerical Methods* John Wiley & Sons, New York (1969).

[4] H. S. Carslaw and J. C. Jaeger, *Conduction of Heat in Solids*, 2nd edition, Oxford University Press, London (1959), URL: https://www.sigmaquadrant.com/product/rare-1959-conduction-of-heat-in-solids-by-h-s-carslaw-j-c-jaeger-2nd-edition/.

[5] A. J. Chamkha, I. V. Miroshnichenko and M. A. Sheremet, Numerical analysis of unsteady conjugate natural convection of hybrid water-based nanofluid in a semicircular cavity, *Journal of Thermal Science and Engineering Applications* **9** (2017), 041004, DOI: 10.1115/1.4036203.

[6] S. K. Das, S. U. Choi, W. Yu and T. Pradeep, *Nanofluids: Science and Technology*, Wiley, Hoboken, (2007), URL: https://www.google.co.in/books/edition/Nanofluids/QpbOpMSpXpYC?hl=en&gbpv=1

[7] S. S. U. Devi and S. P. A. Devi, Numerical investigation of three-dimensional hybrid Cu–Al$_2$O$_3$/water nanofluid flow over a stretching sheet with effecting Lorentz force subject to Newtonian heating, *Canadian Journal of Physics* **94**(5) (2016), 490 – 496, DOI: 10.1139/cjp-2015-0799.

[8] P. Ganesan and H. P. Rani, Transient natural convection along vertical cylinder with heat and mass transfer, *Heat and Mass Transfer* **33** (1998), 449 – 455, DOI: 10.1007/s002310050214.

[9] R. S. R. Gorla, S. Siddiqa, M. A. Mansour, A. M. Rashad and T. Salah, Heat source/sink effects on a hybrid nanofluid-filled porous cavity, *Journal of Thermophysics and Heat Transfer* **31**(4) (2017), 847 – 857, DOI: 10.2514/1.T5085.

[10] T. Hayat and S. Nadeem, Heat transfer enhancement with Ag–CuO/water hybrid nanofluid, *Results in Physics* **7** (2017), 2317 – 2324, DOI: 10.1016/j.rinp.2017.06.034.

[11] S. Kakaç and A. Pramuanjaroenkij, Review of convective heat transfer enhancement with nanofluids, *International Journal of Heat and Mass Transfer* **52**(13-14) (2009), 3187 – 3196, DOI: 10.1016/j.ijheatmasstransfer.2009.02.006.

[12] A. Kasaeian, R. Daneshazarian, O. Mahian, L. Kolsi, A. J. Chamkha, S. Wongwises and I. Pop, Nanofluid flow and heat transfer in porous media: A review of the latest developments, *International Journal of Heat and Mass Transfer* **107** (2017), 778 – 791, DOI: 10.1016/j.ijheatmasstransfer.2016.11.074.

[13] J. Lin and H. Yang, A review on the flow instability of nanofluids, *Applied Mathematics and Mechanics* **40** (2019), 1227 – 1238, DOI: 10.1007/s10483-019-2521-9.

[14] P. Loganathan, P. N. Chand and P. Ganesan, Radiation effects on an unsteady natural convective flow of a nanofluid past an infinite vertical plate, *Nano* **8**(1) (2013), 1350001, DOI: 10.1142/S179329201350001X.

[15] S. A. M. Mehryan, F. M. Kashkooli, M. Ghalambaz, A. J. Chamkha, Free convection of hybrid Al$_2$O$_3$-Cu water nanofluid in a differentially heated porous cavity, *Advanced Powder Technology* **28**(9) (2017), 2295 – 2305, DOI: 10.1016/j.apt.2017.06.011.

[16] G. G. Momin, Experimental investigation of mixed convection with water-Al2O3 & hybrid nanofluid in inclined tube for laminar flow, *International Journal of Scientific & Technology Research* **2**(12) (2013), 195 – 202, URL: https://www.ijstr.org/final-print/dec2013/Experimental-Investigation-Of-Mixed-Convection-With-Water-al2o3-Hybrid-Nanofluid-In-Inclined-Tube-For-Laminar-Flow.pdf.

[17] R. Nimmagadda and K. Venkatasubbaiah, Conjugate heat transfer analysis of micro channel using novel hybrid nanofluids (Al$_2$O$_3$ + Ag/Water), *European Journal of Mechanics - B/Fluids* **52** (2015), 19 – 27, DOI: 10.1016/j.euromechflu.2015.01.007.

[18] Md. J. Nine, B. Munkhbayar, M. Sq. Rahman, H. Chung and H. Jeong, Highly productive synthesis process of well dispersed Cu$_2$O and Cu/Cu$_2$O nanoparticles and its thermal characterization, *Materials Chemistry and Physics* **141**(2-3) (2013), 636 – 642, DOI: 10.1016/j.matchemphys.2013.05.032.

[19] A. T. Olatundun and O. D. Makinde, Analysis of Blasius flow of hybrid nanofluids over a convectively heated surface, *Defect and Discusion Forum* **377** (2017), 29 – 41, DOI: 10.4028/www.scientific.net/DDF.377.29.

[20] V. Rajesh, A. J. Chamkha, Ch. Sridevi and A. F. Al-Mudhaf, A numerical investigation of transient MHD free convective flow of a nanofluid over a moving semi-infinite vertical cylinder, *Engineering Computations* **34**(5) (2017), 1393 – 1412, DOI: 10.1108/EC-03-2016-0090.

[21] V. Rajesh, O. A. Beg and M. P. Mallesh, Transient nanofluid flow and heat transfer from a moving vertical cylinder in the presence of thermal radiation: Numerical study, *Proceedings of the Institution of Mechanical Engineers, Part N: Journal of Nanomaterials, Nanoengineering and Nanosystems* **230**(1) (2016), 3 – 16, DOI: 10.1177/1740349914548712.

[22] J. Sarkar, P. Ghosh and A. Adil, A review on hybrid nanofluids: Recent research, development and applications, *Renewable and Sustainable Energy Reviews* **43** (2015), 164 – 177, DOI: 10.1016/j.rser.2014.11.023.

[23] H. Schlichting and K. Gersten, *Boundary-Layer Theory*, Springer-Verlag, New York, (2001), DOI: 10.1007/978-3-642-85829-1.

[24] S. Suresh, K. P. Venkitaraj, P. Selvakumar and M. Chandrasekar, Effect of Al_2O_3–Cu/water hybrid nanofluid in heat transfer, *Experimental Thermal and Fluid Science* **38** (2012), 54 – 60, DOI: 10.1016/j.expthermflusci.2011.11.007.

[25] S. Suresh, K. P. Venkitaraj, P. Selvakumar and M. Chandrasekar, Synthesis of Al_2O_3–Cu/water hybrid nanofluids using two step method and its thermo physical properties, *Colloids and Surfaces A: Physicochemical and Engineering Aspects* **388**(1-3) (2011), 41 – 48, DOI: 10.1016/j.colsurfa.2011.08.005

[26] B. Takabi, A. M. Gheitaghy and P. Tazraei, Hybrid water-based suspension of Al_2O_3 and Cu nanoparticles on laminar convection effectiveness, *Journal of Thermophysics and Heat Transfer* **30**(3) (2016), 523 – 532, DOI: 10.2514/1.T4756.

[27] T. Tayebi and A. J. Chamkha, Natural convection enhancement in an eccentric horizontal cylindrical annulus using hybrid nanofluids, *Numerical Heat Transfer, Part A: Applications – An International Journal of Computation and Methodology* **71** (2017), 1159 – 1173, DOI: 10.1080/10407782.2017.1337990.

[28] R. K. Tiwari and M. K. Das, Heat transfer augmentation in a two-sided lid-driven differentially heated square cavity utilizing nanofluids, *International Journal of Heat and Mass Transfer* **50**(9-10) (2007), 2002 – 2018, DOI: 10.1016/j.ijheatmasstransfer.2006.09.034.

[29] X.-Q. Wang and A. S. Mujumdar, A review on nanofluids — part I: theoretical and numerical investigations, *Brazilian Journal of Chemical Engineering* **25** (2008), 613 – 630, DOI: 10.1590/S0104-66322008000400001.

[30] X.-Q. Wang and A. S. Mujumdar, A review on nanofluids — part II: experiments and applications, *Brazilian Journal of Chemical Engineering* **25** (2008), 631 – 648, DOI: 10.1590/S0104-66322008000400002.

[31] X.-Q. Wang and A. S. Mujumdar, Heat transfer characteristics of nanofluids: a review, *International Journal of Thermal Sciences* **46**(1) (2007), 1 – 19, DOI: 10.1016/j.ijthermalsci.2006.06.010.